

Research Article pubs.acs.org/acscatalysis

Electroreductive C-C Coupling of Furfural and Benzaldehyde on Cu and Pb Surfaces

Jacob Anibal and Bingjun Xu*



Cite This: ACS Catal. 2020, 10, 11643-11653



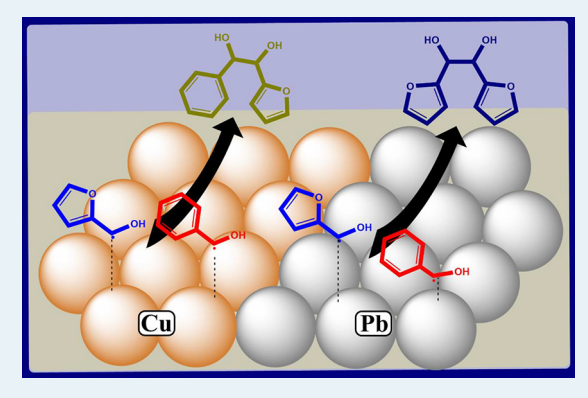
ACCESS I

III Metrics & More



Supporting Information

ABSTRACT: Biomass derived species represent an emerging alternative to petroleum as an industrial carbon feedstock. Effective utilization of biomass requires reductive upgrading of the raw carbon-oxygenates to more valuable compounds. Electroreductive coupling offers a promising strategy for this upgrading by reducing the oxygenated functional groups and increasing molecular weight through C-C bond formation. Despite this promise, elctroreductive coupling suffers from a lack of fundamental understanding. In particular, the cross-coupling of different species remains poorly understood. In this work, the electroreductive coupling of benzaldehyde and furfural on Cu and Pb electrodes is investigated. Reactivity studies show both self-coupling and cross-coupling of the two aldehydes on these two metal surfaces, but with different selectivities. Cu shows greater selectivity for cross-coupling, whereas Pb favors furfural coupling. Comparison with a stochastic model suggests that both metals deviate



from stochastic coupling control, with greater deviation on Pb, likely due to a larger difference in aldehyde binding energies. Cyclic voltammetry (CV) and in situ spectroscopy further support stronger benzaldehyde adsorption compared to furfural on both metals, with a larger difference in binding energy for Pb. Combined, the reactivity, CV, and spectroscopy experiments suggest that crosscoupling of the two aldehydes follows a two reactant Sabatier rule, with optimum cross-coupling for electrodes and similar reactant binding energies.

KEYWORDS: biomass upgrading, C-C coupling, organic electrochemistry

■ INTRODUCTION

Available from sustainable sources, biomass derived carbonoxygenates represent a promising alternative to petroleum as an industrial carbon feedstock. Derived from lignocellulosic materials, these species can be upgraded to form precursors for fuel and chemical production. Typically, this upgrading consists of a reduction to increase stability and energy content, or new C-C bond formation to increase the molecular weight. Often the two processes occur sequentially to form higher value fuels and chemicals.^{2,3} This combined upgrading via coupling and reduction shows particular promise for larger, biomass derived aldehydes, such as benzaldehyde and furfural derivatives. Coupled furfural derivatives, such as furoin, dihydroxymethyl furoin and bihydroxymethyl hydrofuroin, have been demonstrated for C₁₀-C₁₂ biofuel production using sequential ring opening and hydrogenation steps. 4-6 Benzaldehyde derivatives have also been suggested as a potential fuel source following coupling and hydrogenation.⁵ In addition to fuels, coupled furfural and benzaldehyde derivatives also show promise for the production of valueadded products. Mou, Feng, and Chen employed coupled products of hydroxymethyl furfural (HMF) as monomers for the production of polyurethanes. Harvey et al. used coupled

vanillin derivatives to produce renewable thermosetting resins and thermoplastics.8 The promise for valuable precursors also extends to cross-coupled aldehyde species. Recently, Wilson and Chen have synthesized linear polyesters with pendant furan groups using a cross-coupled HMF and furfural species. 5 More generally, the incorporation of different functional groups by cross-coupling presents the opportunity for more valuable dimer products from biomass derived aldehyde species.

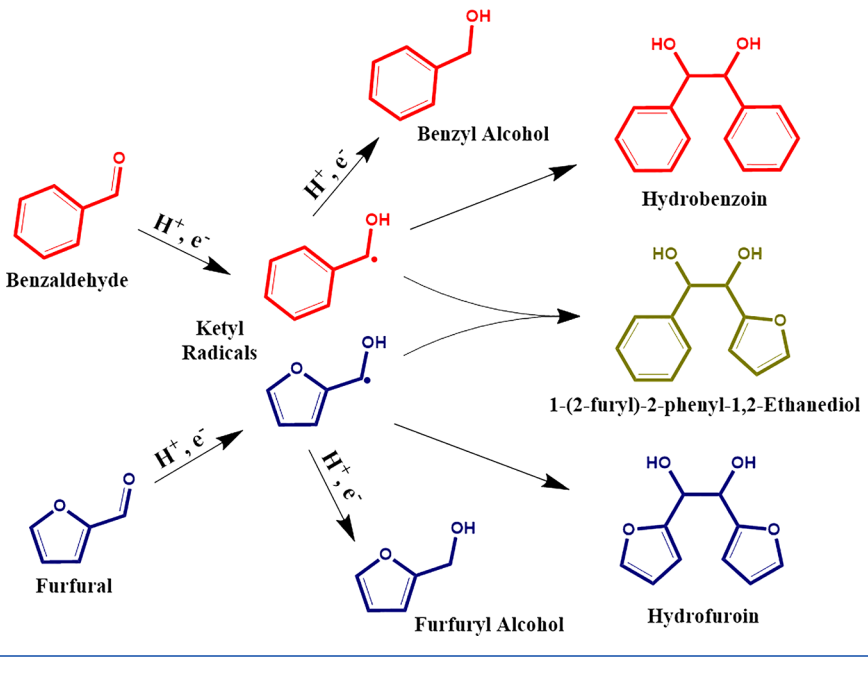
Electroreductive coupling offers a promising means of upgrading biomass derived carbonyl species. Driven by an applied electrical potential, this technique reduces carbonyl species while simultaneously increasing molar mass through new C-C bond formation (dimerization). Generally, electroreductive coupling is considered to proceed by a combination of ketyl radical intermediates, with further reduction to

July 16, 2020 Received: Revised: September 11, 2020 Published: September 11, 2020





Scheme 1. Schematic Representation of the Electrochemical Reduction Pathways for the Mixed Benzaldehyde-Furfural Reduction System



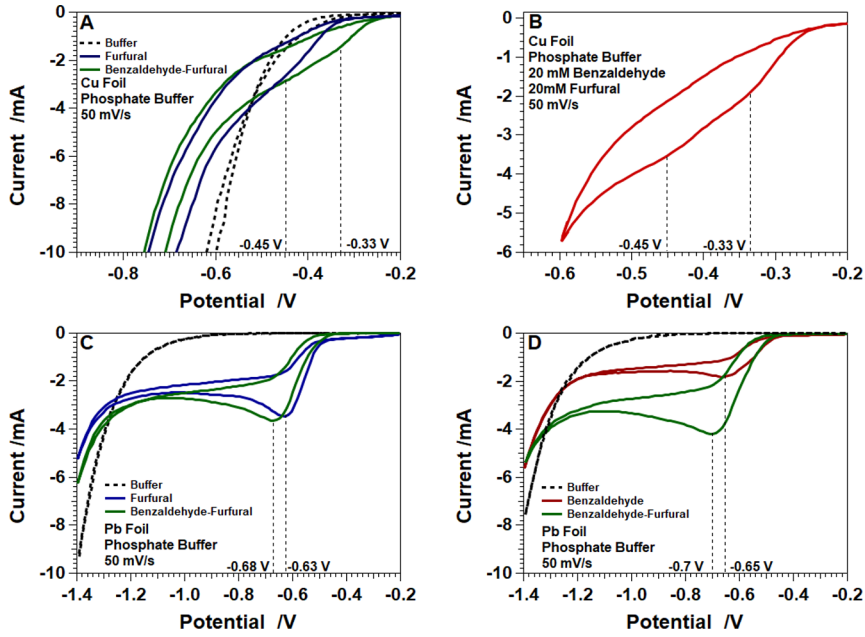


Figure 1. (A) Cyclic voltammograms for furfural and benzaldehyde-furfural solutions on Cu foil. (B) Same as in (A) but with a narrower potential range. (C) Cyclic voltammograms for furfural and benzaldehyde—furfural solutions on Pb foil. (D) Same as in (C) but with benzaldehyde added first then furfural. All voltammograms were collected in pH 6.7 phosphate buffer solution after Ar purge. Benzaldehyde and furfural both had a concentration of 20 mM.

alcohols as an alternate reduction pathway.^{10–14} The two reductions occur sequentially, with an initial electron transfer to form ketyl radicals, followed by either radical coupling or a second, one-electron reduction to an alcohol (Scheme 1). Electrochemical parameters, such as pH, ^{13,14} catalyst, ^{11,15–22} and potential, ^{11,21,22} control the selectivity of the two pathways. Cross-coupling of different aldehydes can also occur electrochemically.²³ Electroreductive coupling has several advantages as an upgrading technique. The one-step process selectively reduces the aldehyde group, eliminating the ring hydrogenation issues often encountered for benzaldehyde

and furfural derivatives.⁴ Additionally, electrochemical reduction occurs at room temperature, without the need for an external hydrogen source or the additional reagents necessary for thermochemical coupling.^{4–6,24} Despite these advantages, electroreductive carbonyl coupling remains poorly understood. The reaction has been extensively demonstrated for benzaldehyde, ^{11,13,21,25} acetophenone, ^{26–30} furfural, ^{31–36} and hydroxymethyl furfural³⁷ but still lacks fundamental understanding into the effect of electrochemical parameters on dimerization rates and selectivities. However, recent work, ^{11,21} including our own, ²² has begun to address this gap in

understanding, with a focus on variation among catalysts. Cross-coupling remains less understood than self-coupling. To our knowledge, only one study covers the electroreductive cross-coupling of aldehydes, involving benzaldehyde, 4-fluorobenzaldehyde, and benzophenone on Pb.²³ The study suggests stochastic control of dimer product selectivities, with a strong dependence on the reactant concentration. However, the lack of further studies makes it difficult to discern if these insights apply generally. In particular, it remains unclear if stochastic control applies to aldehydes with greater structural dissimilarity than benzaldehyde and 4-fluorobenzaldehyde. Additionally, the exclusive investigation of Pb as a cross-coupling catalyst limits insights into catalyst effects, hindering cross-coupling catalyst design.

In this work, we seek to further understand aldehyde crosscoupling by investigating the reduction of benzaldehydefurfural mixtures on Cu and Pb surfaces. We perform cyclic voltammetry (CV) on Cu and Pb, which show a larger impact of benzaldehyde on the furfural reduction peak for Pb than for Cu, suggesting greater competitive adsorption on Pb. Subsequently, we employ reactivity tests to determine coupling rates and selectivities. Both metals produce a cross-coupled species (1-(2-furyl)-2-phenyl-1,2-ethanediol) in addition to alcohol and homo-dimer products. Cu shows greater dimerization selectivity for cross-coupling, whereas Pb favors furfural coupling. To gain further insight into this selectivity difference, we compare the relative dimerization rates with expectations for the stochastic coupling of the ketyl radicals. Both metals show deviation from stochastic expectations, likely due to overbinding of benzaldehyde radicals, with greater deviation on Pb suggesting a greater difference in radical binding energy. Attenuated total reflection surface enhanced infrared reflection absorption spectroscopy (ATR-SEIRAS) experiment results support the larger binding energy difference on Pb. The spectra show benzaldehyde displacement of furfural on Pb but not Cu. Combined, the CV, reactivity, and spectroscopic evidence suggest that the higher cross-coupling selectivity of Cu results from a greater similarity in the ketyl radical binding energies.

■ RESULTS AND DISCUSSION

Cyclic Voltammetry. Cyclic voltammograms collected for benzaldehyde and furfural suggest a larger difference in aldehyde binding energy on Pb than on Cu. Upon furfural introduction to the phosphate buffer electrolyte (pH = 6.7) with a Cu electrode, a shallow peak appears in the cyclic voltammogram at -0.45 V versus the reversible hydrogen electrode (RHE, all potentials in this work are referenced to the RHE), corresponding to furfural reduction (Figure 1A). Further addition of benzaldehyde to the furfural solution produces a similarly weak peak at -0.33 V for benzaldehyde reduction (Figure 1A and B), in agreement with the reduction peak observed at -0.36 V for benzaldehyde alone (Figure S2). We note that both aldehydes show a single broad reduction peak instead of two distinct peaks for the sequential, one electron reductions observed in acidic electrolytes (Scheme 1). 14,23 This broad peak occurs for benzaldehyde reduction at $pH > 3^{14,23}$ and has been suggested to result from a cathodic shift in the first reduction reaction due to the lower stability of the unprotonated radical. Both aldehydes also severely inhibit hydrogen evolution reaction (HER) activity of Cu upon introduction. A similar inhibition is observed for Pt group metals²⁵ (Figure S3A) and Au (Figure S3B), and suggests site

competition between aldehydes and proton (water) reduction on the Cu surface. Pb shows different CV behavior than Cu. Introduction of furfural to the same electrolyte containing a Pb electrode results in a strong reduction peak at -0.63 V (Figure 1C). The sharper peak likely results from a lack of competing HER activity, which does not appear until approximately -1.1V. Interestingly, unlike Cu, introduction of benzaldehyde to the furfural system on Pb results in a slight deepening of the furfural reduction peak and a cathodic shift to -0.68 V (Figure 1C). This change does not correspond to a benzaldehyde reduction peak, as a weaker reduction peak appears at -0.65 Vfor benzaldehyde alone (Figure 1D). A similar mixed peak appears at -0.7 V when furfural is added to benzaldehyde (Figure 1D). The reduction peak intensity also changes for the mixed system but, importantly, depends on the addition order. The peak for the mixed aldehyde system (\sim -0.7 V) shows a similar intensity as furfural alone (Figure 1C), but a large increase over benzaldehyde alone (Figure 1D). The smaller intensity change for benzaldehyde addition to furfural solution, compared to the reverse sequence, suggests the \sim -0.7 V peak corresponds to furfural reduction shifted cathodically due to the presence of benzaldehyde. This shift likely results from competitive adsorption of benzaldehyde and furfural at the Pb surface. Similar cathodic shifts have been observed in the reduction peaks of organic halides upon halide anion (Cl-, Br-, and I⁻) introduction.³⁸ The strong competitive adsorption on Pb contrasts with a previous cross-coupling investigation in which the addition of 4-fluourbenzaldehdye did not significantly affect benzaldehyde reduction.²³ In that case, the strong structural and electrochemical similarities between the two species (< 0.01 V difference in half wave potential) may explain the negligible effect of species interactions on the reduction. A greater structural difference between furfural and benzaldehyde likely explains the stronger effect of competitive adsorption in the present case. These strong interaction effects on Pb caution that the reduction of mixtures may not always behave as a linear combination of the individual components.

Reactivity Tests. Reactivity tests suggest effective crosscoupling of benzaldehyde and furfural on Cu. One-hour reactivity tests were performed on Cu to evaluate the reduction products of equimolar benzaldehyde and furfural in phosphate buffer (pH 6.7). Five main products were identified by coupled gas chromatography and mass spectrometry: benzyl alcohol, furfuryl alcohol, hydrobenzoin, hydrofuroin, and the crosscoupled diol (1-(2-furyl)-2-phenyl-1,2-ethanediol) (Figures S4-S9, Scheme 1). All three dimers show stereo isomers, with two peaks in the chromatograms (Figure S4). We note that the cross-coupled product may have more than two isomers, suggesting that the observed peaks may represent a convolution of multiple species. Herein, we do not distinguish between stereoisomers; all rates and selectivities reflect the sum of isomers for a given dimer. Cu also shows strong hydrogen production at low potentials due to the HER. In addition to Cu, Au and Pt were also tested for benzaldehydefurfural coupling. Consistent with previous work,²² neither Pt nor Au show any aldehyde coupling activity, producing only alcohols and hydrogen (Figure S10). The two aldehydes show similar reduction rates on both Au and Pt, with Pt generally showing higher activity and a higher onset potential. Au and Pt also produce large amounts of hydrogen, which constitutes the major product for both metals. Given the lack of coupling products, no further analysis is undertaken for Au or Pt.

Reactivity tests suggest a preference for cross-coupling on the Cu surface. The distribution of reduction products on Cu shows a strong potential dependence (Figure 2). At less

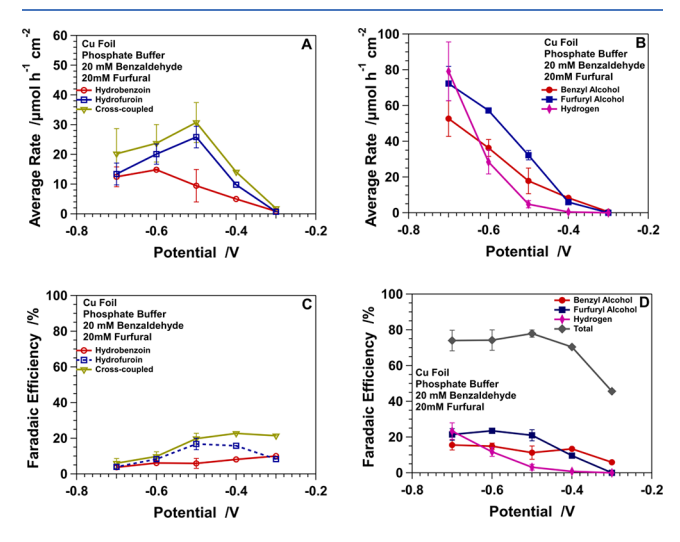


Figure 2. (A) Average reaction rates for the coupled products of furfural and benzaldehyde on Cu foil. (B) Corresponding rates for the alcohol products and hydrogen. (C) FEs for the coupled products. (D) Total FE and efficiencies for hydrogen and the alcohol products. The phosphate buffer consisted of 0.25 M NaH₂PO₄ and 0.25 M Na₂HPO₄ (pH 6.7) and was Ar purged before testing.

negative potential (-0.3 V), benzaldehyde shows slightly higher coupling activity than furfural, with self-dimerization rates of 0.86 and 0.72 μ mol h⁻¹ cm⁻², respectively. This higher benzaldehyde coupling activity agrees with the higher (less cathodic) onset potential observed for benzaldehyde reduction compared to furfural in the cyclic voltammogram on Cu (Figure 1A and B). We note, however, that the higher coupling activity for benzaldehyde is relative to furfural, as the cross-coupled species represents the predominant product at -0.3 V,

with a rate of 1.84 μ mol h⁻¹ cm⁻². At -0.3 V, the reduction also shows greater selectivity toward benzyl alcohol compared to furfuryl alcohol, with a benzyl alcohol rate of 0.50 μ mol h⁻¹ cm⁻² and no detectable furfuryl alcohol. Furfuryl alcohol appears at -0.4 V, although benzyl alcohol still retains the higher rate. Faradaic efficiencies (FEs) mirror the reactivity trends at high potential, with cross-coupling showing the highest FE (Figure 2C). Decreasing the potential results in a transition from dimers to alcohols as the major reduction products (Figure 2). Benzyl alcohol becomes the major selfreduction product for benzaldehyde at -0.4 V with a rate of 8.32 μ mol h⁻¹ cm⁻² compared to 5.01 μ mol h⁻¹ cm⁻² for hydrobenzoin. Furfural reduction transitions slightly lower, at -0.5 V, with rates of 25.8 and 32.2 μ mol h⁻¹ cm⁻² for hydrofuroin and furfuryl alcohol, respectively. The shift from dimer to alcohol agrees with the two sequential reduction steps suggested for benzaldehyde reduction (Scheme 1). 10,13,14,3 Although coproduction of hydrobenzoin and benzyl alcohol at -0.3 V suggests similar reduction potentials for the two steps, as expected from the unresolved peak in the voltammograms (Figure 1A, B and Figure S2). Stepping the potential down (< -0.4 V) also results in a transition from benzaldehyde to furfural as the predominant reduction reaction, with higher rates and FEs for both the alcohol and dimer species (Figure 2). This transition agrees with the CV peak at -0.45 V for furfural (Figure 1A and B) and suggests a more facile reduction for furfural despite its more cathodic onset potential. The higher furfural activity contrasts with recent results for aldehyde reduction on Cu particles, 11,21 which suggest benzaldehyde reduction rates approximately double those of furfural. Although those studies used an 80 mM aldehyde concentration, lower pH, and 47% isopropyl alcohol cosolvent, and these factors could alter relative reduction rates compared to the present study. Dimer production rates also increase with decreasing potential, but at a slowing rate, with all three dimers showing a maximum rate between -0.5 and -0.6 V. This maximum dimerization coincides with a strong rate increase

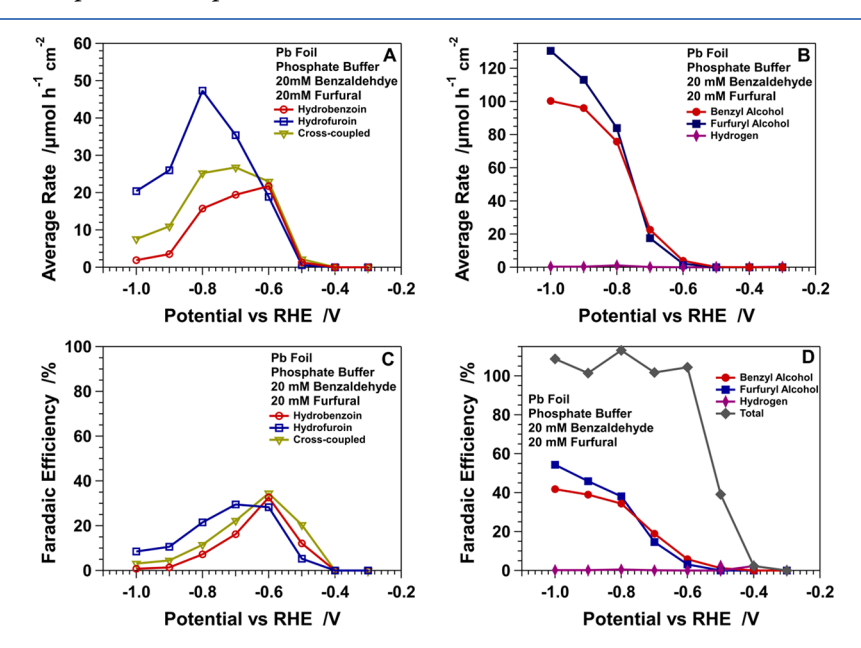


Figure 3. (A) Average reaction rates for the coupled products of furfural and benzaldehyde on Pb foil. (B) Corresponding rates for hydrogen and the alcohols. (C) FEs for the coupled products of benzaldehyde–furfural reduction on Pb. (D) Total FE and efficiencies for the alcohols and hydrogen. The phosphate buffer consisted of 0.25 M NaH₂PO₄ and 0.25 M Na₂HPO₄ (pH 6.7) and was Ar purged before testing.

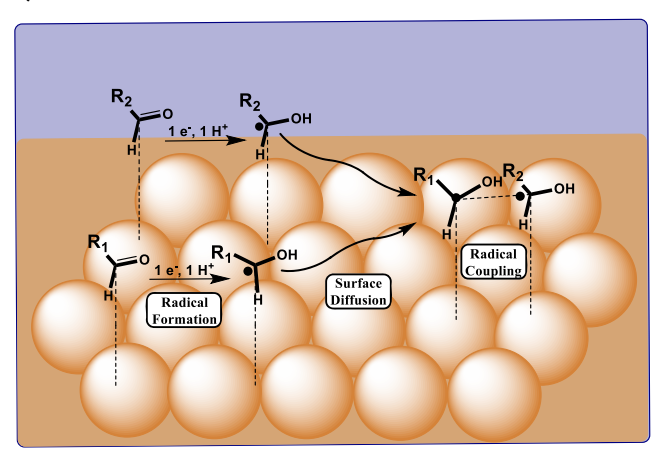
for both alcohols, suggesting that the decline in dimerization results from a lower surface radical concentration due to faster reduction of radicals to alcohols. Alternatively, the lower coupling and higher alcohol activity could result from the reaction of radicals with adsorbed hydrogen species, as the dimerization maximum also appears near the HER onset (Figure 2). This mechanism, effectively a proton coupled electron transfer followed by an inner sphere reaction with adsorbed hydrogen, would also agree with the suppression of furfuryl alcohol production by organothiols on Cu as reported by Chadderdon et al.40 The present data do not provide sufficient evidence to differentiate these two mechanisms. Despite the decline in dimerization, the cross-coupled species remains the predominant dimer at low potentials, with rates ~1.5 times greater than that of hydrofuroin and between 1.5 and 3 times greater than that of hydrobenzoin (Figure S11A). Interestingly, this strong cross-coupling occurs despite a large difference in benzaldehyde and furfural self-coupling rates (Figure 2A). The disparity suggests that the radicals may combine nonstochastically. We discuss this nonstochastic coupling further in the modeling section below. At potentials below -0.7 V, alcohol activity begins to slow with a concurrent increase in the HER activity (Figure 2B and 2D), suggesting competition of the HER with benzaldehyde and furfural reduction. This HER predominance at low potential agrees with previous reactivity studies of furfural reduction. 31,35 Product FEs on Cu (Figure 2C and D) largely parallel the trends in reduction rates (Figure 2A and B). Overall, Cu shows a good total FE, near 80% (Figure 2D). The low FE at −0.3 V results from a low amount of charge passed. Faradaic losses at lower potentials (< -0.3 V) likely result from side reactions of benzaldehyde and furfural to produce larger oligomer species. Such electrochemically generated oligomers have previously been observed for furfural on Cu,31 and we have previously observed similar species for benzaldehyde reduction.²² These oligomer losses suggest practical issues of surface fouling over long time periods, which may be exasperated by running at higher concentrations. 32,36 We note here the possible impact of oligomerization on dimerization selectivity. Preferential electrodimerization of one aldehyde or its products could alter product distributions on Cu. However, benzaldehyde and furfural generally show similar oligomerization selectivities, with FE losses of \sim 20% for benzaldehyde reduction²² and 10– 30% for furfural reduction. 35,40 The similar oligomer losses suggest minimal impact of oligomerization on dimerization selectivities or the k_{ratio} (see below).

Reactivity tests suggest lower cross-coupling selectivity on Pb than on Cu. Pb shows a lower onset potential than Cu, with no detectable products until -0.5 V (Figure 3). To account for this lower onset, the potential window is adjusted, with reactions performed between -0.5 and -1 V. No significant hydrogen production occurs in this region, as expected from the \sim -1.1 V onset observed in the Pb voltammogram (Figure 1C and D). Similar to Cu, the product distribution on Pb shows a strong potential dependence. At high potentials (≥ -0.6 V), the reduction favors dimerization, with slightly higher selectivity toward hydrobenzoin and the cross-coupled species over hydrofuroin. This stronger benzaldehyde coupling supports the higher reduction onset potential for benzaldehyde in the mixed system as inferred from the CV data (Figure 1C and D). Additionally, the dimer predominance agrees with the sequential, one-electron reductions previously suggested for benzaldehyde reduction on Pb. 13,14,23 The presence of benzyl alcohol at $-0.5 \text{ V} (0.13 \ \mu\text{mol h}^{-1} \text{ cm}^{-2})$ does suggest similar reduction potentials for the two steps, similar to the reduction on Cu, in agreement with the voltammograms (Figure 1C and D) and previous reactivity studies. 14,23 Stepping the potential further down results in a transition from benzaldehyde to furfural as the predominant self-coupling reaction and in the predominant reduction path from dimerization to alcohol production. The benzaldehyde to furfural transition occurs sharply between -0.6 and -0.7 V, in agreement with the -0.63 and - 0.68 V reduction peaks observed for benzaldehyde and furfural, respectively, in the Pb voltammograms (Figure 1C and D). Unlike Cu, cross-coupling does not remain dominant after this transition. Instead, hydrofuroin becomes the predominant dimer product at potentials below -0.6 V, with rates 1.3 to 2.7 times higher than the crosscoupled species (Figure 3A and Figure S11B). Benzaldehyde self-coupling again shows the lowest activity, with rates between one half and one tenth those of hydrofuroin (Figure S11B). The strong hydrofuroin activity suggests that the weaker cross-coupling activity does not result from a low furfural radical concentration. Instead, the lower cross-coupling activity (compared to hydrofuroin) likely results from either a low benzaldehyde radical concentration or a smaller rate constant for cross-coupling. The product ratios alone do not provide sufficient information to determine the more likely explanation. However, the stronger benzaldehyde adsorption inferred from the CV data (Figure 1C and D) and spectroscopy (see below) suggests benzaldehyde radicals likely adsorb more strongly than those of furfural, making a low benzaldehyde radical concentration explanation less likely. All three dimers show a maximum rate with potential, with hydrofuroin peaking at a lower potential (-0.8 V) compared to hydrobenzoin and the cross-coupled dimer (-0.6 and -0.7V, respectively). We note that these maxima represent a higher coupling selectivity than Cu. All three dimers show similar maximum FEs, between 29 and 35% (Figure 3C), approximately 10 percentage points higher than the largest coupling FE on Cu (Figure 2C). At -0.6 V, the dimer species combine for 95% FE, highlighting the strong Pb dimerization selectivity at intermediate potentials. Similar to Cu, the dimer maxima on Pb coincide with increasing alcohol rates (Figure 3B), suggesting that the subsequent decrease in dimerization results from greater radical consumption by the alcohol pathway. The alcohol rates continue increasing until -0.9 V at which point they begin to plateau. This plateau likely results from mass transport limitations, as no detectable hydrogen production occurs (Figure 3B). Like the dimer products, the alcohols also show a transition from benzaldehyde to furfural predominance with potential, although the shift occurs at a more cathodic potential (\sim -0.7 V), in agreement with the lower onset potential expected for the second reduction step. Similar to Cu, reduction FEs on Pb reflect the trends in the rate data (Figure 3C and 3D). Overall, Pb also shows better charge balance than Cu, with total efficiencies near 100% for potentials below -0.5V. The higher total FE suggests less electrochemical oligomerization on Pb, although spectroscopic data suggest the surface still fouls through chemical means (see below). Similar to Cu, Pb shows low total efficiencies at high potentials (-0.4 and -0.5 V). These low efficiencies could result from electrochemical oligomerization similar to Cu, although they could also result from errors due to low rates or loss because of the reduction of trace PbO_x on the surface. Given the small amount of charge passed at these potentials (< 2 C) and the

confinement of low FE to high potentials, the latter two explanations appear more likely.

Stochastic Modeling Analysis. Deviation from stochastic control suggests that aldehyde binding energies control coupling selectivities on Cu at low potentials. To gain further insight into cross-coupling selectivity, ratios of the dimer products are compared with those expected from a stochastic model. The model assumes coupling upon the encounter of two radicals, with a first order dependence for each radical (second order overall) and different rate constants for the three coupling reactions. We assume that rate constants may result from either coupling energetics or surface diffusion depending on the rate limiting step (Scheme 2, see the

Scheme 2. Schematic of the Electroreductive Coupling System



Supporting Information for more detailed discussion). Unfortunately, the resulting predictions for dimer ratios depend on the ratio of ketyl radical species coverages at the Cu surface, which remains unknown. Guena and Pletcher²³ circumvented this issue by assuming the radicals had the same ratio as the reactants. In the present case, however, such an assumption seems imprudent given the difference in benzaldehyde and furfural adsorption strength suggested by CV and the spectroscopic data (see below). Fortunately, altering the parameter of interest can circumvent this issue. In particular, we remove radical concentration dependence by taking the ratio of the cross-coupling rate to the geometric average of the self-coupling rates. The resulting parameter, herein termed the k_{ratio}, represents a geometric average of the relative cross-coupling activity compared to furfural and benzaldehyde self-coupling, as in eq 1:

$$k_{\text{ratio}} = \frac{r_{\text{CC}}}{\sqrt{r_{\text{HF}}r_{\text{HB}}}} = \frac{2k_{\text{CC}}C_{\text{F*}}C_{\text{B*}}}{\sqrt{k_{\text{HF}}C_{\text{F*}}^2k_{\text{HB}}C_{\text{B*}}^2}} = \frac{2k_{\text{CC}}}{\sqrt{k_{\text{HF}}k_{\text{HB}}}}$$
(1)

where $r_{\rm CC}$, $r_{\rm HF}$, and $r_{\rm HB}$ are the rates of formation of the cross-coupled dimer, hydrofuroin, and hydrobenzoin, respectively, and $k_{\rm CC}$, $k_{\rm HF}$, and $k_{\rm HB}$ are the rate constants of formation of the cross-coupled dimer, hydrofuroin, and hydrobenzoin, respectively. Eq 1 applies generally for a second order coupling of two radicals, with the rate constants determined either by the energetics of the radical-radical coupling or by the relative diffusion of the reactants (Scheme 2). Assuming a facile coupling step with rates dependent solely on radical concentrations, i.e., a purely stochastic coupling ($k_{\rm CC}=k_{\rm HF}=k_{\rm HB}$), gives a $k_{\rm ratio}$ value of 2. A model based on a modified

Smoluchowski approach $^{41-43}$ suggests that a $k_{\rm ratio}$ of 2 also applies for semistochastic control based on surface diffusion—reaction under certain circumstances (see the Supporting Information for further details). In particular, surface diffusion—reaction approximates stochastic control if the radicals have similar diffusivities and the time scale for diffusion is greater than the radical decomposition time. Rough estimates suggest that these criteria likely apply for the ketyl radical species (see the Supporting Information for further details). We note that the $k_{\rm ratio}$ controls the selectivity of cross-coupling to self-coupling for a given ratio of total radical production rates (Figure 4A) so that a $k_{\rm ratio}$ of 2

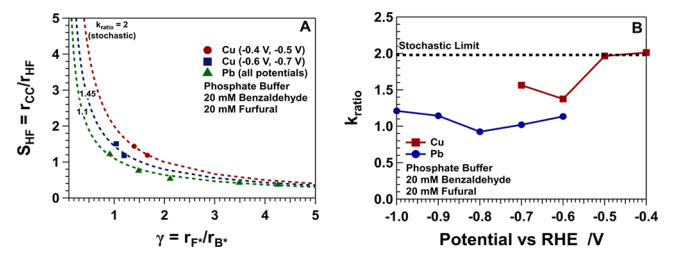


Figure 4. (A) Cross-coupling selectivity (vs hydrofuroin) as a function of $k_{\rm ratio}$ and radical formation ratio for the furfural—benzaldehyde mixtures. The dashed lines are selectivities calculated from the mass balance. (B) $k_{\rm ratio}$ as a function of potential for the reduction of furfural—benzaldehyde mixtures on Cu and Pb foil. The $k_{\rm ratio}$ is defined as the ratio of the cross-coupled dimerization rate to the geometric average of the individual coupling rates (eq 1). The phosphate buffer consisted of 0.25 M NaH₂PO₄ and 0.25 M Na₂HPO₄ (pH 6.7) and was Ar purged before testing.

guarantees stochastic product selectivities (see the Supporting Information for more detail). Deviation of the k_{ratio} from 2, therefore, implies deviation from stochastic coupling. At -0.4and -0.5 V, Cu shows a k_{ratio} of approximately 2 (Figure 4), suggesting stochastically controlled coupling. Reactivity data collected at the most positive potential on Cu and Pb are not included in Figure 4, as the low absolute production rates of dimers result in large uncertainties for their ratios $(r_{\rm CC}/r_{\rm HF})$. At lower potentials, the $k_{\rm ratio}$ on Cu drops, with values of approximately 1.4 and 1.6 at -0.6 and - 0.7 V, respectively (Figure 4). This sharp transition likely results from a change in the rate determining step with potential. For high potentials, the radical formation (first electron transfer) step is likely rate limiting, whereas the coupling step becomes rate limiting at lower potentials. The lower k_{ratio} at lower potential suggests a relatively lower rate for cross-coupling compared to that which the stochastically controlled coupling would entail. This decrease in the relative cross-coupling rate could result from a smaller cross-coupling rate constant compared to furfural coupling, benzaldehyde coupling, or both. Given the larger rate of cross-coupling compared to benzaldehyde coupling (Figure 2A), a smaller cross-coupling rate constant compared to furfural appears more likely. From a physical perspective, this result suggests that the furfural radicals show lower activity in reacting with benzaldehyde radicals than with other furfural radicals. As a necessary corollary, the less active benzaldehyde ketyl radicals would also show lower self-coupling, as observed in the reactivity data (Figure 2A). This difference in radical activity likely results from a difference in radical binding energy. Recent computations have suggested a higher (~0.3 eV) binding energy for benzaldehyde on Cu compared to furfural.¹¹ Assuming a similar difference holds for the radical

species, the stronger binding energy for the benzaldehyde species would explain the lower reduction activity despite the higher onset potential for benzaldehyde (Figure 1A and B). In short, the benzaldehyde species bind too strongly to Cu, resulting in lower coupling activity.

Comparison with the stochastic model suggests the low cross-coupling rate on Pb results from a lower cross-coupling rate constant compared to hydrofuroin. Similar to Cu, comparison of the Pb dimerization data with a stochastic model allows insight into the relative dimerization rates. Unlike Cu, Pb deviates strongly from stochastic control. Below -0.6 V, the k_{ratio} is consistently less than 2 on Pb, with values ranging between 1.25 and 0.9 (Figure 4). The deviation from 2 suggests a lower cross-coupling rate constant compared to either benzaldehyde or furfural self-coupling. Similar to Cu, the lower benzaldehyde coupling rate compared to cross-coupling (Figure 3A and Figure S11B) suggests that the deviation of the k_{ratio} from 2 likely results from a lower cross-coupling rate constant compared to furfural coupling. The lower rate constant has the same interpretation as for Cu, i.e., furfuryl ketyl radicals show greater self-coupling activity compared to coupling with benzaldehyde radicals. This interpretation agrees with the stronger hydrofuroin activity on Pb (Figure 3A). Like Cu, the difference in radical activity likely results from a difference in radical binding energy. The lower k_{ratio} on Pb suggests a greater difference in radical coupling activity and binding energy compared to Cu. This greater binding difference agrees with the greater effect of benzaldehyde on the furfural CV for Pb compared to Cu (Figure 1). Unfortunately, to the authors' knowledge, the binding energies for benzaldehyde and furfural on Pb have not been determined experimentally or computationally, preventing a quantitative comparison. Qualitatively, however, the difference in aldehyde binding energies on Pb appears large given the large difference in coupling selectivities and the furfural peak shift in the cyclic voltammogram. The lower coupling activity for benzaldehyde, despite its stronger binding energy, suggests that benzaldehyde overbinds on both Cu and Pb, with greater overbinding on Pb. Furfural shows more optimal binding, resulting in higher coupling activity. Combined, the two metals suggest that an optimal cross-coupling catalyst requires similar binding energies for the reacting aldehydes.

In Situ Spectroscopic Investigations. In situ spectroscopy supports a difference in aldehyde binding energies on Cu. ATR-SEIRAS is employed to probe the relative adsorption of benzaldehyde and furfural on the Cu surface. To probe relative adsorption strengths, furfural and benzaldehyde are introduced to the Cu surface: first separately, then sequentially. Introduction of furfural to the Cu surface results in new peaks corresponding to furfural (Figure 5A and Figure S13). The peaks at 1567, 1464, and 1395 cm⁻¹ correspond to furan ring modes, while the 1667 and 1369 cm⁻¹ peaks correspond to the C=O stretching and C-H bending modes of the carbonyl, respectively. 44-46 The small peaks at 1667 and 1476 cm⁻¹ correspond to contaminant trans-furfural. 44-46 We note that all identified furfural bands correspond to in-plane vibrations. Generally, the furfural peaks appear close to those of the bulk species (Figure 5A, Figures S13 and S14), suggesting relatively weak furfural adsorption on Cu. Despite the weak adsorption, the furfural peak intensities do show a relative change compared to the bulk species. In particular, the carbonyl (1667 cm⁻¹) peak intensity decreases relative to the other bands. This decrease occurs relatively slowly (~12 min)

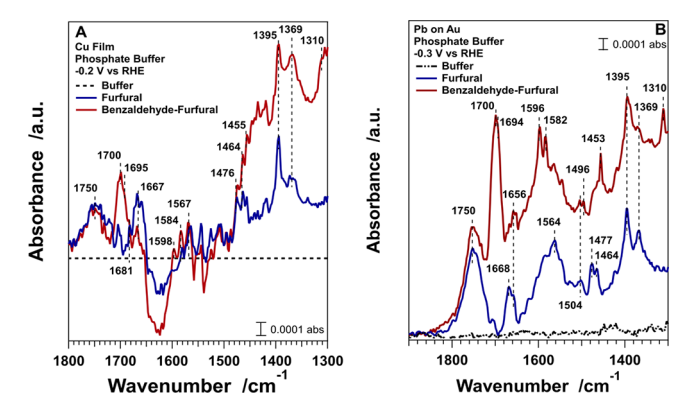


Figure 5. (A) ATR-SEIRAS spectra collected for furfural on a Cu surface before (lower solid trace) and after (upper solid trace) benzaldehyde introduction. (B) ATR-SEIRAS spectra for a furfural-covered Pb surface before (lower solid trace) and after benzaldehyde introduction (upper solid trace). Both aldehydes were added to achieve a 20 mM concentration. All spectra were collected using 64 coadded scans, with 128 background scans. Backgrounds were collected at -0.2 and -0.3 V versus RHE for Cu and Pb, respectively. Phosphate buffer consisted of 0.25 M NaH₂PO₄ and 0.25 M Na₂HPO₄ (pH 6.7) and was Ar purged before testing.

during furfural adsorption (Figure S13) and suggests a concentration dependent reorientation of furfural upon adsorption. Per ATR-SEIRAS surface selection rules, 47,48 the intensity of vibration modes decreases as their dipole moment becomes more parallel to the surface, with no infrared (IR) absorption for vibrations completely parallel to the surface. For furfural, the selection rules suggest that adsorption results in a C=O bond more parallel to the surface than the furan ring vibrations. Furthermore, the decrease of the carbonyl peak with time suggests that the C=O bond becomes more parallel as additional furfural adsorbs. Higher furfural coverage may force furfural to adsorb more perpendicular to the surface to enable closer packing, resulting in a concurrent change in the orientation of the C=O bond (Scheme 3). This interpretation

Scheme 3. Schematic Representation of the Proposed Changes in Furfural Orientation on Cu with Increasing Coverage and Benzaldehyde Adsorption

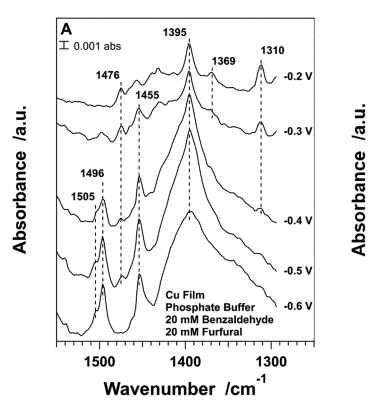
agrees with a study in vacuum suggesting that benzaldehyde undergoes a transition to vertical adsorption with increasing coverage on Pd.⁴⁹ In addition to furfural, a broad peak also appears at 1750 cm⁻¹, developing more slowly with time than the other bands (Figure 5A and Figure S13). Given the peak width and stronger time dependence, the peak likely corresponds to oligomer or decomposition products formed by furfural on the Cu surface. Benzaldehyde introduction to the Cu surface results in peaks consistent with those previously reported for adsorbed benzaldehyde (Figure S15).²² Peaks at 1598, 1584, 1455, and 1310 cm⁻¹ correspond to the ring

modes of benzaldehyde. 50 The peak at 1706 cm⁻¹ corresponds to the carbonyl stretch of bulk benzaldehyde, with a shoulder at 1695 cm⁻¹ corresponding to the carbonyl of the adsorbed benzaldehyde species. ^{22,51,52} Like furfural, all observed benzaldehyde bands correspond to in-plane vibrations. Unlike furfural, benzaldehyde does not show an appreciable change in carbonyl peak intensity upon adsorption or with adsorption time (Figure S15), suggesting a similar orientation of the carbonyl and ring modes. To probe relative binding strengths and coadsorption effects, benzaldehyde is introduced to a furfural covered Cu surface (Figure 5A). As expected, benzaldehyde peaks appear at 1700, 1598, 1584, 1455, and 1310 cm⁻¹, similar to benzaldehyde on Cu (Figure S15). We note that the peak frequencies typically vary by ± 2 cm⁻¹ between tests. In addition to benzaldehyde peak emergence, furfural carbonyl peak intensity decreases with benzaldehyde introduction. Similar to furfural adsorption (Figure S13), this decrease in carbonyl intensity does not coincide with a decrease in any other furfural band, suggesting reorientation, not displacement, of furfural. The C-H aldehyde bending peak (1369 cm⁻¹) actually increases upon benzaldehyde adsorption. Combined, these changes suggest that benzaldehyde adsorption likely causes a similar reorientation as that observed during the adsorption of furfural on Cu, forcing the furfural into a vertical adsorption with the C=O nearly parallel to the surface (Scheme 3). The reorientation, rather than displacement, of furfural by benzaldehyde suggests only marginally stronger binding for benzaldehyde. This slightly stronger benzaldehyde binding agrees with the calculated binding energies, 11 as well as the negligible effect of benzaldehyde on the furfural voltammogram (Figure 1A). Additionally, the furfural reorientation supports the assignment of the aldehyde peaks to adsorbed species, as bulk spectra would add linearly and not result in a peak decrease.

Benzaldehyde introduction results in more effective displacement of furfural on Pb, suggesting a greater difference in aldehyde binding energies compared to Cu. The introduction of furfural to the Pb surface results in similar peaks as on Cu, with major peaks at 1668, 1564, 1476, 1464, 1395, and 1369 cm⁻¹ (Figure 5B and Figure S16). The carbonyl peak position shows greater variation (\pm 5 cm⁻¹) than the other furfural peaks due to interference from the adjacent water band (Figure 5B and Figure S16). Similar to Cu, the carbonyl peak for furfural decreases over time during adsorption (Figure S16) while the other peaks remain nearly constant, suggesting reorientation of furfural with increasing coverage. Pb also shows an oligomer/decomposition peak at 1750 cm⁻¹. The peak appears larger (relative to the furfural bands) than that on Cu, suggesting greater furfural oligomerization and/or decomposition on Pb. Benzaldehyde on Pb also shows similar peaks as Cu, with bands at 1694, 1596, 1582, 1453, and 1310 cm⁻¹ (Figure S17). We note that the contribution of the bulk benzaldehyde band (1700-1706 cm⁻¹) varies between tests (Figure 5B and Figure S17) due to film damage during the plating process. Similar to Cu, the benzaldehyde carbonyl peak does not decrease during adsorption on Pb, suggesting minimal reorientation. The benzaldehyde spectra on Pb also show a broad peak at 1389 cm⁻¹ (Figure S17). This peak likely corresponds to an adsorbed benzoate species, given its similar position and width to benzoate observed on Au²² and likely results from the reaction of benzaldehyde with trace PbO_x on the surface. We note here the possible impact of the Au underlayer on the Pb spectra. Previous work has shown

benzaldehyde adsorption on Au, 22 with similar peak locations as observed on Pb and Cu. However, two considerations suggest a negligible effect of the Au underlayer in the present case. First, the current decay observed during plating (Figure S1) suggests nearly complete Pb coverage, with minimal Au exposure. Second, the spectroscopic observation of dimer species for the Pb film (see below) supports a predominantly Pb surface, as these species do not appear on Au spectroscopically²² or in reactivity tests (Figures S10A and S10C). Combined, these considerations suggest that the Pb films represent a Pb surface, with minimal interference from the Au underlayer. The main difference between Pb and Cu appears upon sequential aldehyde addition. Introducing benzaldehyde to the furfural covered Pb surface results in a decrease in the furfural carbonyl band (Figure 5B). Unlike Cu, however, the other furfural bands also decrease, although not as drastically as the carbonyl peak. The more general decrease in furfural intensity suggests greater displacement of furfural by benzaldehyde on Pb, likely due to a larger difference in aldehyde binding energies for the Pb surface. This greater binding difference agrees with the stronger effect of benzaldehyde on the furfural CV for Pb (Figure 1C and D) and the lower k_{ratio} (Figure 4). The stronger benzaldehyde binding also likely applies to its ketyl radical intermediate, supporting different radical binding energies as an explanation for the different coupling selectivities on Cu and Pb. On both surfaces, stronger benzaldehyde binding makes a lower benzaldehyde radical concentration unlikely and suggests that the difference in dimerization rates results from different radical binding energies. Furthermore, the increase in the aldehyde binding energy difference from Cu to Pb corresponds to a decrease in cross-coupling selectivity. This inverse correlation of binding energy difference and cross-coupling selectivity suggests that overbinding of benzaldehyde (relative to furfural) limits cross-coupling, as well as benzaldehyde selfcoupling, on both surfaces, with Pb showing greater overbinding of benzaldehyde than Cu. In short, the combined reactivity and spectroscopic data suggest cross-coupling follows a two reactant Sabatier rule, with the difference in aldehyde binding energy controlling the relative rates of cross-coupling and self-coupling.

Benzaldehyde shows a greater impact on furfural reduction for Pb than Cu, supporting stronger relative benzaldehyde binding on the Pb surface. The potential of the Cu surface is stepped down to observe surface adsorbates under reduction conditions. Upon stepping the potential down, additional peaks appear at 1505, 1496, and 1455 cm⁻¹ for the benzaldehyde-furfural mixture (Figure 6A and Figure S18). We note that the 1455 cm⁻¹ peak overlaps with the benzaldehyde peak at the same wavenumber. However, as no other benzaldehyde peaks increase with the potential, the 1455 cm⁻¹ peak largely results from a new species. The peaks at 1496 and 1455 cm⁻¹ correspond to both hydrobenzoin and benzyl alcohol, as these bands overlap for the two species.⁵³ Both peaks have been previously observed for benzaldehyde reduction on Cu²² and appear for the reduction of benzaldehyde alone (Figure \$19). The peak at 1505 cm⁻¹ corresponds to a furfural reduction product, as it also appears for furfural reduction on Cu (Figure S20). Given the peak size, and the lack of a peak near 1380 cm⁻¹ expected for furfuryl alcohol, 53 the 1505 cm⁻¹ peak likely corresponds to hydrofuroin. This assignment agrees with the spectrum collected for synthesized hydrofuroin in acetonitrile (Figure S21). We note



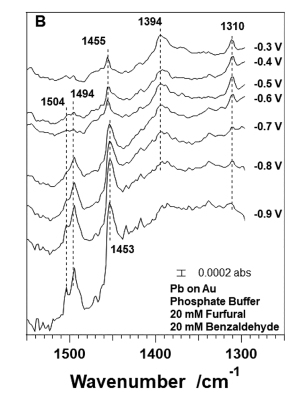


Figure 6. (A) Spectra collected for equimolar benzaldehyde and furfural under reduction conditions on Cu. (B) Same, but for a Pb surface. All spectra were collected using 64 coadded scans, with 128 background scans. Backgrounds were collected at -0.2 and -0.3 V versus RHE for Cu and Pb, respectively. The phosphate buffer consisted of 0.25 M NaH₂PO₄ and 0.25 M Na₂HPO₄ (pH 6.7). The buffer was Ar purged before testing.

that no distinct peak appears for the cross-coupled species despite its predominance in the reactivity tests (Figure 2A and C). The lack of this peak could result from two possibilities. First, the cross-coupled species may have a distinct peak between the two individual product peaks which remain unresolved. This explanation appears unlikely given its predominance in the product distribution. Alternatively, the two moieties of the cross-coupled species may have relatively independent vibrational modes, resulting in two peaks for the cross-coupled species at nearly identical frequencies as hydrobenzoin and hydrofuroin. This explanation appears more likely given the negligible effect of the additional phenyl ring on the hydrobenzoin peak position compared to benzyl alcohol.⁵³ The spectra collected during the coelectrolysis of benzaldehyde and furfural also lack any distinguishable feature for benzaldehyde or furfural ketyl radical species (Figure 6A). The lack of radical peaks could result from the higher rate of radical consumption in the present case, with total dimerization rates 3.5 times larger than those of the previous work under acidic conditions (pH 4.6).²² Alternatively, the smaller difference in aldehyde and radical reduction potentials at higher pH^{14,23} may play a role by limiting the potential window in which radicals predominate. In addition to growth in product peaks, the reactant peaks decrease at lower potentials. This decrease suggests some mass transport limitations for the spectroscopic cell, as it coincides with the reduction onset (-0.3 to -0.4 V, Figures 2 and 6A). Importantly, neither the reactant nor product peaks show any shift in position with potential, i.e., a Stark tuning effect (Figure 6A, Figure S18-S20). The lack of Stark tuning suggests these species adsorb outside the inner Helmholtz layer which contains the strong electric field required for Stark tuning.⁵ This layer has been estimated as 2 to 4 Å thick, based on CO Stark tuning rates^{54,55} and X-ray scattering of cations.^{56,57} The relatively distant adsorption of the benzaldehyde and furfural species suggest relatively weak interaction with the Cu surface. Although the different Cu and Pb reduction rates and selectivities suggest an appreciable effect of surface interaction on the reduction. Stepping the potential down on Pb gives spectra similar to Cu, but with different onset potentials (Figure 6B, Figures S22 and S23). On Pb, benzaldehyde introduction suppresses furfural reduction at high potentials

and shifts the appearance of furfural products ~200 mV cathodically (Figure 6B and Figure S22). Although weak dimer peaks still appear at higher potentials (Figure 6B). This cathodic shift agrees with the effect of benzaldehyde on the furfural CV (Figure 1C and 1D) and suggests stronger competitive adsorption for benzaldehyde species on Pb. The stronger competitive adsorption supports greater benzaldehyde overbinding on Pb as the cause of lower cross-coupling selectivity, as inferred from the stochastic modeling and benzaldehyde displacement data. Importantly, this stronger adsorption remains nonspecific. No detectable Stark tuning occurs on Pb (Figure 6B, Figures S22 and S23), suggesting that the variation in dimerization selectivities between Pb and Cu does not result from greater specific adsorption on Pb.

CONCLUSIONS

Effective cross-coupling of benzaldehyde and furfural has been demonstrated on Cu and Pb foil. Of the two, Cu shows a higher selectivity toward the cross-coupled species, while Pb favors furfural dimerization. For both metals, dimerization occurs at high potentials, with a transition to alcohol production at lower potentials. Cyclic voltammograms show a larger impact of benzaldehyde on furfural reduction for the Pb surface, suggesting a larger difference in aldehyde binding energy on Pb. Analysis of relative dimerization rates suggests that the difference in radical binding energies may explain the difference in dimerization selectivities. In particular, the $k_{\rm ratio}$ (cross-coupling rate over geometric average of the selfcoupling rates) has been demonstrated as a useful parameter to characterize relative dimerization rates independent of intermediate concentrations. In situ ATR-SEIRAS spectra show greater furfural displacement by benzaldehyde on Pb, supporting a greater aldehyde binding energy difference for the Pb surface. Both surfaces show IR peaks for hydrofuroin, hydrobenzoin, and benzyl alcohol under reduction conditions. Combined, the voltammetry, reactivity, and spectroscopic data suggest that benzaldehyde-furfural cross-coupling follows a two-reactant Sabatier rule, with the difference in ketyl radical binding energy controlling the cross-coupling selectivity of a catalyst. This rule likely applies to other cross-coupling systems and the difference in radical binding energy may provide a design criterion for further development of cross-coupling catalysts.

ASSOCIATED CONTENT

Supporting Information

The Supporting Information is available free of charge at https://pubs.acs.org/doi/10.1021/acscatal.0c03110.

Experimental Section; CV data; product identification information; modeling derivations; ATR-SIERAS spectra (PDF)

AUTHOR INFORMATION

Corresponding Author

Bingjun Xu — Center for Catalytic Science and Technology,
Department of Chemical and Biomolecular Engineering,
University of Delaware, Newark, Delaware 19716, United
States; College of Chemistry and Molecular Engineering, Peking
University, Beijing 100871, China; orcid.org/0000-00022303-257X; Email: bxu@udel.edu

Author

Jacob Anibal — Center for Catalytic Science and Technology, Department of Chemical and Biomolecular Engineering, University of Delaware, Newark, Delaware 19716, United States

Complete contact information is available at: https://pubs.acs.org/10.1021/acscatal.0c03110

Notes

The authors declare no competing financial interest.

ACKNOWLEDGMENTS

This work is supported by the National Science Foundation CAREER Program (Award No. CBET-1651625).

REFERENCES

- (1) Huber, G. W.; Iborra, S.; Corma, A. Synthesis of Transportation Fuels from Biomass: Chemistry, Catalysts, and Engineering. *Chem. Rev.* **2006**, *106*, 4044–4098.
- (2) Cho, H. J.; Kim, D.; Li, J.; Su, D.; Xu, B. Zeolite-Encapsulated Pt Nanoparticles for Tandem Catalysis. J. Am. Chem. Soc. 2018, 140, 13514–13520.
- (3) Cho, H. J.; Kim, D.; Li, S.; Su, D.; Xu, B. Molecular-Level Proximity of Metal and Acid Sites in Zeolite- Encapsulated Pt Nanoparticles for Selective Multistep Tandem Catalysis. *ACS Catal.* **2020**, *10*, 3340–3348.
- (4) Wegenhart, B. L.; Yang, L.; Kwan, S. C.; Harris, R.; Kenttämaa, H. I.; Abu-Omar, M. M. From Furfural to Fuel: Synthesis of Furoins by Organocatalysis and Their Hydrodeoxygenation by Cascade Catalysis. *ChemSusChem* **2014**, *7*, 2742–2747.
- (5) Huang, Y. B.; Yang, Z.; Dai, J. J.; Guo, Q. X.; Fu, Y. Production of High Quality Fuels from Lignocellulose-Derived Chemicals: A Convenient C-C Bond Formation of Furfural, 5-Methylfurfural and Aromatic Aldehyde. *RSC Adv.* **2012**, *2*, 11211–11214.
- (6) Liu, D.; Chen, E. Y. X. Diesel and Alkane Fuels from Biomass by Organocatalysis and Metal-Acid Tandem Catalysis. *ChemSusChem* **2013**, *6*, 2236–2239.
- (7) Mou, Z.; Feng, S.; Chen, E. Y. X. Bio-Based Difuranic Polyol Monomers and Their Derived Linear and Cross-Linked Polyurethanes. *Polym. Chem.* **2016**, *7*, 1593–1602.
- (8) Harvey, B. G.; Guenthner, A. J.; Meylemans, H. A.; Haines, S. R. L.; Lamison, K. R.; Groshens, T. J.; Cambrea, L. R.; Davis, M. C.; Lai, W. W. Renewable Thermosetting Resins and Thermoplastics from Vanillin. *Green Chem.* **2015**, *17*, 1249–1258.
- (9) Wilson, J. F.; Chen, E. Y. X. Difuranic Diols for Renewable Polymers with Pendent Furan Rings. *ACS Sustainable Chem. Eng.* **2019**, *7*, 7035–7046.
- (10) Rusling, J. F.; Segretario, J. P.; Zuman, P. Polarographic Reduction of Aldehydes and Ketones. *J. Electroanal. Chem. Interfacial Electrochem.* **2006**, 143, 291–321.
- (11) Lopez-Ruiz, J. A.; Andrews, E. M.; Akhade, S. A.; Lee, M.; Koh, K.; Sanyal, U.; Yuk, S. F.; Karkamkar, A. J.; Derewinski, M. A.; Holladay, J.; Glezakou, V.; Rousseau, R.; Gutiérrez, O. Y.; Holladay, J. D. Understanding the Role of Metal and Molecular Structure on the Electrocatalytic Hydrogenation of Oxygenated Organic Compounds. *ACS Catal.* **2019**, *9*, 9964–9972.
- (12) Lopez-Ruiz, J. A.; Sanyal, U.; Egbert, J.; Gutiérrez, O. Y.; Holladay, J. Kinetic Investigation of the Sustainable Electrocatalytic Hydrogenation of Benzaldehyde on Pd/C: Effect of Electrolyte Composition and Half-Cell Potentials. ACS Sustainable Chem. Eng. 2018, 6, 16073–16085.
- (13) Birkett, M. D.; Kuhn, A. T. The Electrochemical Reduction of Benzaldehyde. *Electrochem. Acta* 1980, 25, 273–278.
- (14) Guena, T.; Pletch, D. Electrosyntheses from Aromatic Aldehydes in a Flow Cell. Part I. The Reduction of Benzaldehyde. *Acta Chem. Scand.* **1998**, *52*, 23–31.

- (15) Udhayan, R.; Basheer Ahamed, K. A. Electrochemical Reduction of Carbonyl Compounds. B. Electrochem 1988, 141, 163–12078.
- (16) Chen, Y. L.; Chou, T. C. Electrochemical Reduction of Benzaldehyde Using Ag/Nafion as an Electrode. *Ind. Eng. Chem. Res.* **1994**, 33, 676–680.
- (17) Polcaro, A. M.; Palmas, S.; Dernini, S. Electrochemical Reduction of Carbonyl Compounds at Modified Carbon Felt Electrodes. *Electrochim. Acta* 1993, 38, 199–203.
- (18) Durant, A.; François, H.; Reisse, J.; Kirsch-DeMesmaeker, A. Sonoelectrochemistry: The Effects of Ultrasound on Organic Electrochemical Reduction. *Electrochim. Acta* 1996, 41, 277–284.
- (19) Chiba, T.; Okimoto, M.; Nagai, H.; Takata, Y. Electrocatalytic Reduction Using Raney Nickel. *Chem. Soc. Japan* **1982**, *56*, 719–723.
- (20) Udupa, H. V. K.; Subramanian, G. S.; Udupa, K. S.; Natarajan, K. A Comparative Study of the Reduction of Aromatic Aldehydes at Stationary and Rotating Amalgamated Cathodes. *Electrochim. Acta* 1964, 9, 313–323.
- (21) Andrews, E. M.; Lopez-Ruiz, J. A.; Egbert, J. D.; Koh, K.; Sanyal, U.; Song, M.; Li, D.; Karkamkar, A. J.; Derewinski, M. A.; Holladay, J. E.; Gutiérrez, O. Y.; Holladay, J. D. Performance of Base and Noble Metals for Electrocatalytic Hydrogenation of Bio-Oil-Derived Oxygenated Compounds. ACS Sustainable Chem. Eng. 2020, 8, 4407–4418.
- (22) Anibal, J.; Malkani, A.; Xu, B. Stability of the Ketyl Radical as a Descriptor in the Electrochemical Coupling of Benzaldehyde. *Catal. Sci. Technol.* **2020**, *10*, 3059–3194.
- (23) Guena, T.; Pletch, D. Electrosyntheses from Aromatic Aldehdyes in a Flow Cell. Part II. The Crosscoupling of Benzaldehydes Unsymmetrical Diols. *Acta Chem. Scandanavia* 1998, 52, 32–36.
- (24) Zang, H.; Wang, K.; Zhang, M.; Xie, R.; Wang, L.; Chen, E. Y. X. Catalytic Coupling of Biomass-Derived Aldehydes into Intermediates for Biofuels and Materials. *Catal. Sci. Technol.* **2018**, *8*, 1777–1798.
- (25) Song, Y.; Sanyal, U.; Pangotra, D.; Holladay, J. D.; Camaioni, D. M.; Gutiérrez, O. Y.; Lercher, J. A. Hydrogenation of Benzaldehyde via Electrocatalysis and Thermal Catalysis on Carbon-Supported Metals. *J. Catal.* **2018**, *359*, 68–75.
- (26) Villalba, M.; Del Pozo, M.; Calvo, E. J. Electrocatalytic Hydrogenation of Acetophenone and Benzophenone Using Palladium Electrodes. *Electrochim. Acta* **2015**, *164*, 125–131.
- (27) Chen, B. L.; Xiao, Y.; Xu, X. M.; Yang, H. P.; Wang, H.; Lu, J. X. Alkaloid Induced Enantioselective Electroreduction of Acetophenone. *Electrochim. Acta* **2013**, *107*, 320–326.
- (28) Sáez, A.; García-García, V.; Solla-Gullón, J.; Aldaz, A.; Montiel, V. Electrochemical Synthesis at Pre-Pilot Scale of 1-Phenylethanol by Cathodic Reduction of Acetophenone Using a Solid Polymer Electrolyte. *Electrochem. Commun.* **2013**, *34*, 316–319.
- (29) Nakahara, K.; Naba, K.; Saitoh, T.; Sugai, T.; Obata, R.; Nishiyama, S.; Einaga, Y.; Yamamoto, T. Electrochemical Pinacol Coupling of Acetophenone Using Boron-Doped Diamond Electrode. *ChemElectroChem* **2019**, *6*, 4153–4157.
- (30) Rudd, E. J.; Conway, B. E. Elementry Steps and the Solvent Effect in Electrochemical Reduction of Acetophenone. *Trans. Faraday Soc.* **1971**, *67*, 440–457.
- (31) Jung, S.; Biddinger, E. J. Electrocatalytic Hydrogenation and Hydrogenolysis of Furfural and the Impact of Homogeneous Side Reactions of Furanic Compounds in Acidic Electrolytes. *ACS Sustainable Chem. Eng.* **2016**, *4*, 6500–6508.
- (32) May, A. S.; Biddinger, E. J. Strategies to Control Electrochemical Hydrogenation and Hydrogenolysis of Furfural and Minimize Undesired Side Reactions. *ACS Catal.* **2020**, *10*, 3212–3221.
- (33) Nilges, P.; Schröder, U. Electrochemistry for Biofuel Generation: Production of Furans by Electrocatalytic Hydrogenation of Furfurals. *Energy Environ. Sci.* **2013**, *6*, 2925–2931.

- (34) Cao, Y.; Noël, T. Efficient Electrocatalytic Reduction of Furfural to Furfuryl Alcohol in a Microchannel Flow Reactor. *Org. Process Res. Dev.* **2019**, 23, 403–408.
- (35) Jung, S.; Biddinger, E. J. Controlling Competitive Side Reactions in the Electrochemical Upgrading of Furfural to Biofuel. *Energy Technol.* **2018**, *6*, 1370–1379.
- (36) Albert, W.; Lowy, A. The Electrochemical Reduction of Furfural. *Trans. Electrochem. Soc.* **1939**, *75*, 367–375.
- (37) Roylance, J. J.; Kim, T. W.; Choi, K. S. Efficient and Selective Electrochemical and Photoelectrochemical Reduction of 5-Hydroxymethylfurfural to 2,5-Bis(Hydroxymethyl)Furan Using Water as the Hydrogen Source. ACS Catal. 2016, 6, 1840–1847.
- (38) Ardizzone, S.; Cappelletti, G.; Mussini, P. R.; Rondinini, S.; Doubova, L. M. Adsorption Competition Effects in the Electrocatalytic Reduction of Organic Halides on Silver. *J. Electroanal. Chem.* **2002**, 532, 285–293.
- (39) Zuman, P. Topics in Organic Polarography; Plenum Publishing Company: Newyork, NY, 1970.
- (40) Chadderdon, X. H.; Chadderdon, D. J.; Matthiesen, J. E.; Qiu, Y.; Carraher, J. M.; Tessonnier, J. P.; Li, W. Mechanisms of Furfural Reduction on Metal Electrodes: Distinguishing Pathways for Selective Hydrogenation of Bioderived Oxygenates. *J. Am. Chem. Soc.* **2017**, 139, 14120–14128.
- (41) Smoluchowski, M. V. Zur kinetischen Theorie der Transpiration und Diffusion verdünnter Gase. *Ann. Phys.* **1915**, 338, 129–1570. (42) Collins, F.; Kimball, G. Diffusion-Controlled Reaction Rates. *J.*
- Colloid Sci. 1949, 4, 425-437.
- (43) Freeman, D. L.; Doll, J. D. The Influence of Diffusion on Surface Reaction Kinetics. *J. Chem. Phys.* **1983**, *78*, 6002–6009.
- (44) Rico, M.; Barrachina, M.; Orza, J. M. Fundamental Vibrations of Furan and Deuterated Derivatives. *J. Mol. Spectrosc.* **1967**, 24, 133–148.
- (45) Adamek, P.; Volka, K.; Ksandr, Z.; Stibor, I. Vibrational Spectra of 2-Furaldehyde. J. Mol. Spectrosc. 1973, 47, 252–267.
- (46) Thompson, H. W.; Temple, R. B. Infra-Red Spectra of Furan and Thiophen. *Trans. Faraday Soc.* **1944**, *41*, 27–34.
- (47) Hatta, A.; Ohshima, T.; Suëtaka, W. Observation of the Enhanced Infrared Absorption of P-Nitrobenzoate on Ag Island Films with an ATR Technique. *Appl. Phys. A Solids Surfaces* **1982**, 29, 71–75
- (48) Greenler, R. G.; Snider, D. R.; Witt, D.; Sorbello, R. S. The Metal-Surface Selection Rule for Infrared Spectra of Molecules Adsorbed on Small Metal Particles. *Surf. Sci.* **1982**, *118*, 415–428.
- (49) Pang, S. H.; Román, A. M.; Medlin, J. W. Adsorption Orientation-Induced Selectivity Control of Reactions of Benzyl Alcohol on Pd(111). *J. Phys. Chem. C* **2012**, *116*, 13654–13660.
- (50) Zwarich, R.; Smolarek, J.; Goodman, L. Assignment of Out-of-Plane Vibrational Modes in Benzaldehyde. *J. Mol. Spectrosc.* **1971**, 38, 336–357.
- (51) Keresszegi, C.; Ferri, D.; Mallat, T.; Baiker, A. Unraveling the Surface Reactions during Liquid-Phase Oxidation of Benzyl Alcohol on Pd /Al2O3: An in Situ ATR-IR Study. *J. Phys. Chem. B* **2005**, *109*, 958–967.
- (52) Ferri, D.; Mondelli, C.; Krumeich, F.; Baiker, A. Discrimination of Active Palladium Sites in Catalytic Liquid-Phase Oxidation of Benzyl Alcohol. *J. Phys. Chem. B* **2006**, *110*, 22982–22986.
- (53) NIST Spectrometry Data Center. In NIST Chemistry WebBook, NIST Standard Reference Database Number 69; Linstrom, P. J., Mallard, W. G.; National Institute of Science and Technology: Gaithersburg, MD 2018.
- (54) Lambert, D. K. Vibrational Stark Effect of CO on Ni(100), and CO in the Aqueous Double Layer: Experiment, Theory, and Models. *J. Chem. Phys.* **1988**, *89*, 3847–3860.
- (55) Lambert, D. K. Vibrational Stark Effect of Adsorbates at Electrochemical Interfaces. *Electrochim. Acta* **1996**, 41, 623–630.
- (56) Strmcnik, D.; Van Der Vliet, D. F.; Chang, K. C.; Komanicky, V.; Kodama, K.; You, H.; Stamenkovic, V. R.; Marković, N. M. Effects of Li+, K+, and Ba2+ Cations on the ORR at Model and High Surface

- Area Pt and Au Surfaces in Alkaline Solutions. J. Phys. Chem. Lett. 2011, 2, 2733–2736.
- (57) Lucas, C. A.; Thompson, P.; Gründer, Y.; Markovic, N. M. The Structure of the Electrochemical Double Layer: Ag(111) in Alkaline Electrolyte. *Electrochem. Commun.* **2011**, *13*, 1205–1208.